

## Inorganic Chemistry | Hot Paper |

Binary Lead Fluoride Pb<sub>3</sub>F<sub>8</sub>

H. Lars Deubner<sup>+, [a]</sup>, Malte Sachs<sup>+, [a]</sup>, Jascha Bandemehr,<sup>[a]</sup> Sergei I. Ivlev,<sup>[a]</sup> Antti J. Karttunen,<sup>[b]</sup> Stefan R. Kachel,<sup>[a]</sup> Benedikt P. Klein,<sup>[a]</sup> Lukas Ruppenthal,<sup>[a]</sup> Maik Schöniger,<sup>[a]</sup> Claudio K. Krug,<sup>[a]</sup> Jan Herritsch,<sup>[a]</sup> J. Michael Gottfried,<sup>[a]</sup> Jamal N. M. Aman,<sup>[c]</sup> Jörn Schmedt auf der Günne,<sup>[c]</sup> and Florian Kraus\*<sup>[a]</sup>

**Abstract:** The binary lead fluoride Pb<sub>3</sub>F<sub>8</sub> was synthesized by the reaction of anhydrous HF with Pb<sub>3</sub>O<sub>4</sub> or by the reaction of BrF<sub>3</sub> with PbF<sub>2</sub>. The compound was characterized by single-crystal and powder X-ray diffraction, IR, Raman, and solid-state MAS <sup>19</sup>F NMR spectroscopy, as well as thermogra-

vimetric analysis, XP and near-edge X-ray absorption fine structure (NEXAFS) spectroscopy. Solid-state quantum-chemical calculations are provided for the vibrational analyses and band assignments. The electronic band structure offers an inside view of the mixed valence compound.

## Introduction

The binary lead fluorides PbF<sub>2</sub> and PbF<sub>4</sub> are well established compounds.<sup>[1,2]</sup> Their first lab synthesis dates back to the first half of the 19th century and the determination of their crystal structures to 1944 and 1962, respectively.<sup>[1–4]</sup> In addition, PbF<sub>3</sub>, which is better described as Pb<sub>2</sub>F<sub>6</sub> containing Pb<sup>II</sup> and Pb<sup>IV</sup> atoms, was reported.<sup>[5]</sup> While for Sn and Ge also the mixed valence compounds M<sub>3</sub>F<sub>8</sub> (M=Sn, Ge), and even Ge<sub>5</sub>F<sub>12</sub> and Ge<sub>7</sub>F<sub>16</sub> are known, only the three binary lead fluorides mentioned above are unambiguously known.<sup>[6–9]</sup> Therefore, the existence of a mixed valence compound of the composition Pb<sub>3</sub>F<sub>8</sub> appears to be likely. For lead, mixed valence compounds are nothing special and the well-characterized compound Pb<sub>3</sub>O<sub>4</sub> (*latin*: Minium), which was used as a pigment in ancient Rome and in anti-corrosion coatings, or which is even today in usage for charlatanism, comes to the mind.<sup>[10–13]</sup> A compound of the average chemical composition {Pb<sub>3</sub>F<sub>8</sub>} was mentioned

only twice in the literature. Nothing besides this average composition has been reported. Pb<sub>3</sub>F<sub>8</sub> was first mentioned in 1972 by Banner and co-workers as a result of the reaction of Pb<sub>3</sub>O<sub>4</sub> with gaseous HF on a thermogravimetric scale.<sup>[14]</sup> In their search for Pb<sub>2</sub>F<sub>6</sub>, Charpin and co-workers described reactions leading to Pb<sub>3</sub>F<sub>8</sub> as a product or side product. Again, no details on Pb<sub>3</sub>F<sub>8</sub> were given, even not how the compound was identified as Pb<sub>3</sub>F<sub>8</sub>.<sup>[15]</sup> Herein, we present the synthesis and characterization of the binary lead(II/IV) fluoride Pb<sub>3</sub>F<sub>8</sub>.

## Results and Discussion

The formation of the title compound can be envisaged by the following stoichiometric Equation (1).




Pb<sub>3</sub>O<sub>4</sub> is reacted with an excess of anhydrous HF (aHF) at room temperature, so that the equilibrium of the reaction is shifted to the product side. After a few minutes of reaction time the deep-orange color of Pb<sub>3</sub>O<sub>4</sub> is already gone and the reaction is complete within one hour at room temperature. After the removal of the volatiles (HF and H<sub>2</sub>O), the product is obtained as a slightly beige powder (Figure S1, Supporting Information) that is easily ground. The dry powder of Pb<sub>3</sub>F<sub>8</sub> is stable for several hours in air. The compound prepared in this way always contains small amounts of PbF<sub>2</sub> (typically 5–8%), as evidenced by Rietveld analysis (Table S1, Figure S2, Supporting Information) on powder X-ray diffraction patterns. The obtained lattice parameters are  $a=8.8434(1)$ ,  $b=7.5427(1)$ ,  $c=10.2339(1)$  Å,  $\beta=98.810(1)^\circ$ ,  $V=672.3(3)$  Å<sup>3</sup> at  $T=298$  K. They agree well with those obtained from single-crystal X-ray diffraction, see below. To suppress the back reaction by hydrolysis, a large excess of circa 100 equivalents of aHF is needed. If the reaction mixture is allowed to stand for three days at room temperature, or, if an excess of aHF is used that is too small, a


[a] Dipl.-Chem. H. L. Deubner,<sup>+</sup> M. Sachs,<sup>+</sup> J. Bandemehr, Dr. S. I. Ivlev, S. R. Kachel, B. P. Klein, L. Ruppenthal, M. Schöniger, C. K. Krug, J. Herritsch, Prof. Dr. J. M. Gottfried, Prof. Dr. F. Kraus  
Fachbereich Chemie, Philipps-Universität Marburg  
Hans-Meerwein-Str. 4, 35032 Marburg (Germany)  
E-mail: florian.kraus@chemie.uni-marburg.de

[b] Prof. Dr. A. J. Karttunen  
Department of Chemistry and Materials Science  
Aalto University, 00076 Aalto (Finland)

[c] J. N. M. Aman, Prof. Dr. J. Schmedt auf der Günne  
Inorganic Materials Chemistry, University of Siegen  
Adolf-Reichwein-Str. 2, 57076 Siegen (Germany)

[\*] These authors contributed equally.

 Supporting information and the ORCID identification number(s) for the author(s) of this article can be found under:  
<https://doi.org/10.1002/chem.201903954>.

 © 2019 The Authors. Published by Wiley-VCH Verlag GmbH & Co. KGaA. This is an open access article under the terms of the Creative Commons Attribution License, which permits use, distribution and reproduction in any medium, provided the original work is properly cited.

product is obtained that always contains larger amounts of  $\text{PbF}_2$  than mentioned above. To obtain phase pure  $\text{Pb}_3\text{F}_8$  we attempted to oxidize  $\text{PbF}_2$  using an excess of  $\text{BrF}_3$  under warming up to  $130^\circ\text{C}$ . However, after evaporation of the residual  $\text{BrF}_3$ , the remaining colorless powder consists of  $\text{Pb}_3\text{F}_8$  and small amounts of  $\text{Pb}_2\text{F}_6$  (circa 3%). Thermogravimetric investigations (Figures S3, S4, Supporting Information, and for further details see the Supporting Information) indicate that the thermal decomposition of  $\text{Pb}_3\text{F}_8$  is complex. The decomposition under loss of fluorine gas starts roughly around  $80^\circ\text{C}$ . After thermal decomposition, pure  $\text{PbF}_2$  is obtained as evidenced by powder XRD (Figure S5, Supporting Information). The overall mass loss during this procedure has been determined twice, once to 5.2 and once to 4.7%. Both values are in reasonably good agreement with the theoretically expected mass loss of 4.9%. Thus,  $\text{Pb}_3\text{F}_8$  decomposes thermally to three equivalents of  $\text{PbF}_2$  and one equivalent of  $\text{F}_2$ . Further details will be reported elsewhere. Helium pycnometric density determination (see the Supporting Information) yields a density of circa  $7.68\text{ g cm}^{-3}$  for the used sample of  $\text{Pb}_3\text{F}_8$ . Due to the presence of circa 15%  $\text{PbF}_2$  ( $\rho=8.44\text{ g cm}^{-3}$ ) in the sample used for density determination, a value of  $7.74\text{ g cm}^{-3}$  is to be expected from the measurements. Thus, the experimentally determined density is in very good agreement with the measurement and with the crystallographic density of  $\text{Pb}_3\text{F}_8$  of circa  $7.61\text{ g cm}^{-3}$ .

Single-crystal X-ray diffraction shows  $\text{Pb}_3\text{F}_8$  to crystallize in the monoclinic space group  $I2/a$  (No. 15,  $mS44$ ,  $15ef^5$ ) with the lattice parameters  $a=8.7800(18)$ ,  $b=7.4927(15)$ ,  $c=10.196(5)\text{ \AA}$ ;  $\beta=98.78(3)^\circ$ ;  $V=662.9(4)\text{ \AA}^3$ ;  $Z=4$ , at  $T=100\text{ K}$ , while at room temperature lattice parameters of  $a=8.8400(5)$ ,  $b=7.5398(5)$ ,  $c=10.2297(7)\text{ \AA}$ ,  $\beta=98.82(2)^\circ$ ,  $V=673.77(8)\text{ \AA}^3$  are obtained. The latter agree well with the values determined from powder X-ray diffraction at room temperature. No phase change was observed upon cooling from room temperature to  $100\text{ K}$  and Table S2, Supporting Information, holds details of the single crystal structure determination. Surprisingly,  $\text{Pb}_3\text{F}_8$  is not isotypic to the compounds  $M_3\text{F}_8$  ( $M=\text{Ge}, \text{Sn}$ ) but, to the best of our knowledge, represents a novel structure type.<sup>[6,7]</sup> As the crystal structure of  $\text{Pb}_3\text{F}_8$  is complicated we will start with the local structure description before we describe it globally. There are two types of Pb atoms, Pb(1) and Pb(2). The Pb(1) atoms (Wyckoff position 4e) are coordinated by F atoms (8f) in the shape of an irregular octahedron, while the coordination polyhedron around the Pb(2) atom (8f) reminds of a pentagonal pyramid (Figure 1).

All F atoms around the Pb(1) atom are  $\mu_2$ -bridging to Pb(2) atoms. The Pb(1)–F atomic distances are observed in the range from  $2.048(3)$  to  $2.063(3)\text{ \AA}$ . They agree well with reported ones for hexafluoridoplumbates(IV) in compounds such as  $M^{\text{II}}\text{PbF}_6$  ( $M^{\text{II}}=\text{Mg}$  ( $1.99\text{ \AA}$ ),  $\text{Ni}$  ( $1.99\text{ \AA}$ ),  $\text{Zn}$  ( $1.97\text{ \AA}$ ),  $\text{Sr}$  ( $2.042$ – $2.060\text{ \AA}$ ),  $\text{Ba}$  ( $2.04\text{ \AA}$ ),  $\text{Pb}$  ( $1.991$ – $2.011\text{ \AA}$ )) or  $M^{\text{I}}\text{PbF}_6$  ( $M^{\text{I}}=\text{Ag}$  ( $2.021$ – $2.100\text{ \AA}$ ),  $\text{Li}$  ( $1.997\text{ \AA}$ )), which however all contain spatially separated  $[\text{PbF}_6]^{2-}$  octahedra.<sup>[16–20]</sup> Therefore, we assign oxidation state +IV to these octahedron-like coordinated Pb(1) atoms. As stated above, the Pb(2) atoms are coordinated by six fluorine atoms in a shape similar to a pentagonal pyramid (Figure 1) and the Pb(2)–F distances span a rather broad range

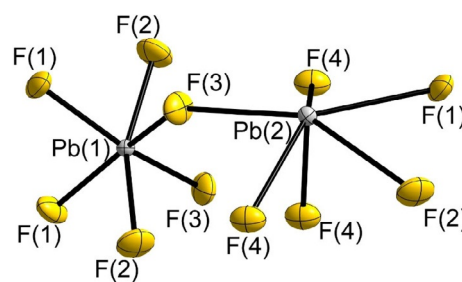


**Figure 1.** The coordination spheres of the two lead atoms of  $\text{Pb}_3\text{F}_8$ . The Pb(1) atom is coordinated octahedron-like, the Pb(2) atom like a pentagonal pyramid. Pb atoms are shown in grey, F atoms in yellow. Displacement ellipsoids at 70% probability at  $100\text{ K}$ .

from  $2.330(3)$  to  $2.651(3)\text{ \AA}$ . As they are clearly longer than the Pb(1)–F distances, we assign oxidation state +II to the Pb(2) atoms. Charge distribution (CHARDI) calculations<sup>[21]</sup> (Table S3, Supporting Information) agree with the description of  $\text{Pb}_3\text{F}_8$  as a mixed valence compound as charges of +4.12 and +1.94 are calculated for the Pb(1) and Pb(2) atoms, respectively. Thus, the assignment of the oxidation states is supported.

One Pb(2)–F(4) distance within the pentagonal pyramid is shortest with  $2.330(3)\text{ \AA}$ , and represents the “tip” of the pyramid pointing to the bottom in Figure 1. The other two Pb(2)–F(4) distances are longer and equal within the standard uncertainty ( $2.446(3)$  and  $2.449(3)\text{ \AA}$ ). The other Pb(2)–F distances are significantly longer and range from  $2.505(3)$  to  $2.651(3)\text{ \AA}$ . As can be seen in Figure 1, the Pb(2) atom is not located in the center of the coordination polyhedron but resides close to the pentagonal face. Such a coordination polyhedron is reminiscent of the text-book anion  $[\text{XeOF}_5]^-$ ,<sup>[22–24]</sup> and the peculiar location and coordination sphere of the Pb(2) atom is attributed to an accumulation of electron density in real space as shown in the quantum chemical calculations below. Due to the chemical hardness of the fluoride anion and its extremely low polarizability, its electron density leads to repulsion and deformation of the electron density at the Pb atom. Some call this effect the “sterically active lone-pair” and its influence on local as well as crystal structure is known for example from  $\alpha$ - and  $\beta$ - $\text{PbO}$ , or from the black and pigeon blood red modifications of  $\text{SnO}$ .<sup>[25–27]</sup> However, above the “lone-pair” of the  $\text{Pb}^{\text{II}}$  atom there are three additional F atoms with Pb–F distances of  $2.851(4)$ ,  $2.874(3)$ , and  $3.051(3)\text{ \AA}$ . According to the distance histogram one could count those three F atoms to the coordination sphere of Pb(2) leading to coordination number  $6+3$ . The coordination polyhedron around Pb(2) is then irregular with ten triangles and one tetragon as the faces. Also, the calculated effective coordination number (ECoN) of 6.9 hints to a small contribution of the three next-nearest fluorine atoms to its coordination sphere, whereas the calculated ECoN for Pb(1) agrees well with C. N.=6 as assigned by our structure analysis.

We will now come to the global structure description by explaining how the coordination polyhedra are interconnected. The F(4) atoms are  $\mu_3$ -bridging between Pb(2) atoms and that leads to the formation of a 1D infinite zigzag ladder shown in Figure 2a. The two longer Pb(2)–F(4) distances form the stringers of the ladder, while the short Pb(2)–F(4) distances represent

the rungs of the ladder (Figure 2a). Thus, the “lone-pairs” on the Pb(2) atoms point to the left and right in Figure 2a.

The topside and underside of the infinite ladder are coordinated by  $[\text{Pb}(1)\text{F}_6]^{2-}$  octahedra as shown in Figure 2b. The ladders are sandwiched between the octahedra and vice versa, leading to a 2D infinite layer of ladders interconnected by octahedra. A section is shown in Figure 3a.

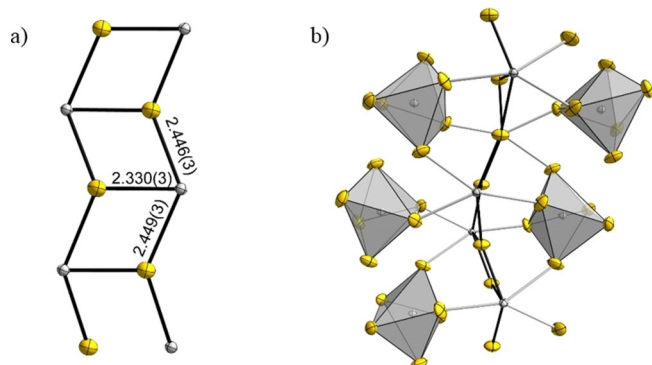


**Figure 2.** a) Ladder-like connection of the Pb(2) atoms (grey) via  $\mu_3$ -bridging F(4) atoms (yellow). b) Connection of the Pb(2) containing ladder to the Pb(1) containing octahedra. Displacement ellipsoids shown with 70% probability at 100 K.

Thus, the “sterically active lone-pairs” of the Pb(2) atoms point out of the topside and underside of these layers (Figure 3b) separating them from each other. Figure 3b shows a section of the crystal structure of  $\text{Pb}_3\text{F}_8$  with the 2D infinite layers parallel to the *ab* plane stacked along the *c* axis. The *Niggli* formula indicates the coordination number and environment of the Pb atoms nicely. For the Pb<sup>II</sup> atom  $[\text{PbF}_{3/2}\text{F}_{3/3}]$  and for the Pb<sup>IV</sup> atom  $[\text{PbF}_{6/2}]$  is obtained. Thus,  $\text{Pb}_3\text{F}_8$  can be described by the *Niggli* formula  ${}^2_{\infty}[\text{PbF}_{3/2}\text{F}_{3/3}]_2[\text{PbF}_{6/2}]$ . The Pb atoms are hexagonally packed and each is anticuboctahedrally surrounded by twelve Pb atoms. Thus, the arrangement of the Pb atoms of  $\text{Pb}_3\text{F}_8$  corresponds to the simple Mg structure type. However, the F atoms neither fill the octahedral nor the tetrahedral voids of the sphere packing.

Raman spectroscopic investigations have been carried out on  $\text{Pb}_3\text{F}_8$  and on  $\text{PbF}_2$  for comparison. For experimental details

see the Supporting Information. The experimentally obtained spectra were then compared with ones obtained from DFT-PBE0/TZVP calculations based on the crystal structures of  $\text{Pb}_3\text{F}_8$  and  $\text{PbF}_2$ . The most striking difference between the Raman spectrum of  $\text{Pb}_3\text{F}_8$  and the spectrum of  $\text{PbF}_2$  (see Figures S6 and S7, Supporting Information) is the strong vibrational band at  $531\text{ cm}^{-1}$  that is only present in the Raman spectrum of  $\text{Pb}_3\text{F}_8$ . This band is well reproduced by our theoretical findings and can be attributed to a symmetric stretching of the  $\text{Pb}^{\text{IV}}\text{-F}$  bonds, which explains the absence of this band in  $\text{PbF}_2$ .  $\text{Pb}_3\text{F}_8$  is also clearly identified by the lattice vibrational bands around  $100\text{ cm}^{-1}$  as this frequency region corresponds to a minimum in Raman intensity in the spectrum of  $\text{PbF}_2$ . The two peaks at around  $250\text{ cm}^{-1}$  and the two peaks at around  $200\text{ cm}^{-1}$  belong to a symmetric stretching of the  $\text{Pb}^{\text{II}}\text{-F}$  bonds and bending modes of the  $\text{Pb}^{\text{IV}}\text{-F}$  bonds, respectively. In summary, the Raman spectrum supports our classification of  $\text{Pb}_3\text{F}_8$  as a mixed valence compound. Full band assignments are available from Tables S4 to S6, Supporting Information.

An IR spectroscopic investigation of  $\text{Pb}_3\text{F}_8$  powder in the range from  $4000$  to  $450\text{ cm}^{-1}$  (Figure S8) shows only a single broader band at  $466\text{ cm}^{-1}$ , which is comprised of intense  $\text{Pb}^{\text{IV}}\text{-F}$  stretch and weaker  $\text{Pb}^{\text{II}}\text{-F}$  scissoring and rocking modes. For  $\text{Li}_2\text{PbF}_6$ , which contains  $[\text{PbF}_6]^{2-}$  octahedra, a band at  $475\text{ cm}^{-1}$  has been observed.<sup>[16]</sup> This agrees well considering the different connectivity of the  $[\text{PbF}_6]^{2-}$  octahedra in the two compounds. The experimentally determined band position of  $\text{Pb}_3\text{F}_8$  agrees well with the quantum chemically calculated bands at  $493$ ,  $470$ , and  $456\text{ cm}^{-1}$ . The complete assignment of IR bands is given in Table S5, Supporting Information. The obtained  $\text{Pb}_3\text{F}_8$  is essentially free of impurities such as  $\text{H}_2\text{O}$ ,  $\text{OH}^-$ , or  $\text{HF}$ , as no bands in the range from  $4000$  to circa  $450\text{ cm}^{-1}$  are present.

Solid-state  $^{19}\text{F}$  MAS NMR experiments (Figure 4 and Table 1) of  $\text{Pb}_3\text{F}_8$  were performed to further corroborate the crystal structure model. The  $^{19}\text{F}$  DEPTH MAS NMR spectrum shows four resonances, one occurring at  $\delta = -18.2\text{ ppm}$  and a group of three overlapping signals at  $\delta = -40$ ,  $-48.5$ , and  $-56\text{ ppm}$ . All four resonances have peak areas including spinning sidebands of 1:0.84:1.03:0.90. The spectrum also contains a fifth peak at  $\delta = -24.2\text{ ppm}$  with a lower intensity which is likely to originate from the  $\text{PbF}_2$  impurity.<sup>[28]</sup> These observations are expected for F atoms which do not have fast ion-dynamics on

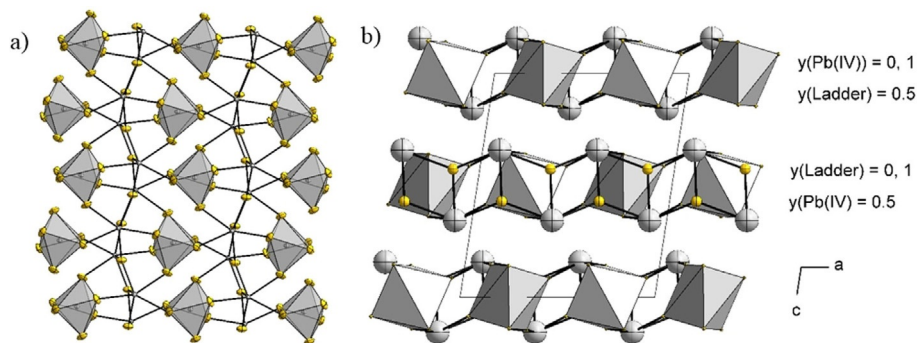


**Figure 3.** a) A part of the 2D infinite layer formed by the sandwiching of  $[\text{Pb}(1)\text{F}_6]^{2-}$  octahedra by Pb(2) containing ladders. Displacement ellipsoids at 70% probability at 100 K. b) A section of the crystal structure of  $\text{Pb}_3\text{F}_8$ . Atoms are shown isotropic with arbitrary radii. Pb atoms grey, F atoms yellow. The 2D infinite layers run parallel to the *ab* plane. The height along the *b* axis is shown with the approximate *y* coordinate of the gravimetric center of the building units.

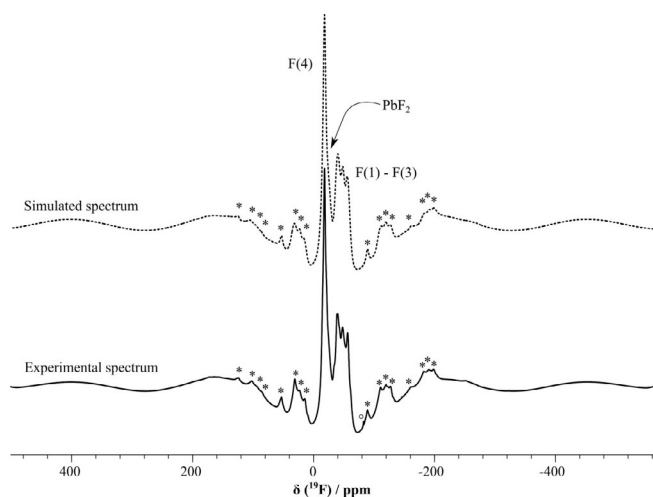


**Figure 4.**  $^{19}\text{F}$  DEPTH MAS NMR spectrum (experimental: solid line, simulated: dashed line) of  $\text{Pb}_3\text{F}_8$  at 20 kHz spinning frequency. The spinning side bands are marked with asterisks. The simulation includes a version of the DEPTH<sup>[32,33]</sup> sequence with four  $\pi$ -pulses:  $\pi/2$ - $\pi$ - $\pi$ - $\pi$ - $\tau_{\text{deadtime}}$ -FID. The DEPTH experiment results in MAS NMR spectra free of probe head background. The simulation includes the effect of the deadtime delay and excitation profile of the DEPTH sequences which causes the baseline rolling. Zeroth and first order phase correction are included as variable parameters in the least-square fit.

**Table 1.** Estimates for the  $^{19}\text{F}$  solid-state NMR chemical shift parameters for  $\text{Pb}_3\text{F}_8$  obtained by a least-square fit of the experimentally obtained spectrum (Figure 4) with SIMPSON version 3.1.2<sup>[29]</sup> simulations of the used version of the DEPTH<sup>[30,31]</sup> experiment.

Site	$\delta_{\text{iso}}$ [ppm]	$\delta_{\text{aniso}}$ [ppm]	$\eta$	$\delta_{11}$ [ppm]	$\delta_{22}$ [ppm]	$\delta_{33}$ [ppm]
F(4)	-18.2	66.1	0.60	47.9	-31.5	-71.2
F(1)-F(3)	-40.0	-111.8	0.61	50.5	-18.5	-151.7
F(1)-F(3)	-48.5	-121.0	0.65	51.5	-27.4	-169.5
F(1)-F(3)	-56.0	-119.2	0.47	31.6	-24.5	-175.2

the NMR timescale, as four symmetry-inequivalent F atoms (F(1) to F(4)) with the same site multiplicity are present in the crystal structure.

A tentative peak assignment of the  $^{19}\text{F}$  resonances follows the idea that neighboring cations contribute to the  $^{19}\text{F}$  chemical shift according to their coordination number and distance to F atoms in ionic fluorides.<sup>[32]</sup> Consequently, F atoms with a similar bonding situation should feature similar isotropic and anisotropic chemical shift values. In the present case (Table 1) the group of three resonances has an anisotropic chemical shift which is larger by about a factor of two compared to the peak which appears at the highest ppm values. In the structure three F atoms are coordinated to two Pb atoms, one F atom is coordinated to three. Therefore, the resonance at -18.2 ppm is assigned to the three-fold coordinated fluorine site (F(4)) and the three signals at -40, -48.5, and -56 ppm are assigned to the fluorine atoms F(1), F(2), and F(3) coordinated by the two lead Pb(1) and Pb(2) atoms.

We have performed X-ray photoelectron spectroscopy (XPS) as well as near-edge X-ray absorption fine structure (NEXAFS) measurements to get information about the electronic structure of  $\text{Pb}_3\text{F}_8$ . The survey XP spectrum of  $\text{Pb}_3\text{F}_8$  on carbon tape is presented in Figure 5a. The spectrum only shows contributions from Pb and F atoms, besides minor C 1s and O 1s peaks from the carbon tape.

Another sample that was studied with hard X-ray photoelectron spectroscopy (HAXPES, Figure S9 in the Supporting Information) shows the same features and even less contributions from the carbon tape. During the XPS and HAXPES measurements, the sample exhibits substantial photoemission-induced charging, which results in peak shifts and broadening. For this reason, a refined analysis of the XPS peak shapes with a discrimination between  $\text{Pb}^{\text{II}}$  and  $\text{Pb}^{\text{IV}}$  contributions is not possible. Instead, we performed NEXAFS spectroscopy measurements on the Pb  $M_5$ -edge to gain further insight into the electronic structure of  $\text{Pb}_3\text{F}_8$  (Figure 5c). As a reference, we also studied  $\text{PbF}_2$  and  $\text{Pb}_3\text{O}_4$ . Between 2490 and 2495 eV, a pre-edge feature is observed, which is followed by the  $M_5$ -edge for all three species.  $\text{PbF}_2$  shows a sharp peak at 2490 eV with a minimum at 2495 eV. In contrast, there is only a broad feature between 2490 and 2495 eV for  $\text{Pb}_3\text{O}_4$ . The  $\text{Pb}_3\text{F}_8$  spectrum resembles a mixture of both reference samples. A peak at 2490 eV is observed, whereas there is no minimum at 2495 eV like for  $\text{PbF}_2$ .

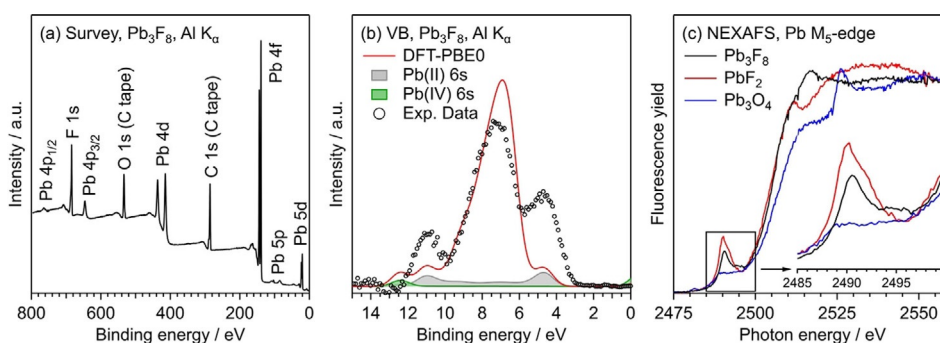


**Figure 5.** (a) Survey XP spectrum of  $\text{Pb}_3\text{F}_8$  on carbon tape, taken with monochromatic  $\text{Al K}\alpha$  radiation. (b) Valence band spectrum of  $\text{Pb}_3\text{F}_8$  measured with  $\text{Al K}\alpha$  radiation in comparison to DFT calculations (PBE0/NCPW). A Shirley background was subtracted from the experimental data to compare it to the theoretical results. The contribution of the Pb 6s orbitals to the total calculated DOS is highlighted. Further details concerning the data treatment are given in the Supporting Information. (c) Pb  $M_5$ -edge NEXAFS spectra of  $\text{Pb}_3\text{F}_8$ ,  $\text{PbF}_2$  and  $\text{Pb}_3\text{O}_4$  measured by the X-ray fluorescence yield. Inset: Zoom-in of the pre-edge feature.

Instead, there is a broad feature similar to the case of  $\text{Pb}_3\text{O}_4$ . This is in line with the presence of both  $\text{Pb}^{\text{II}}$  and  $\text{Pb}^{\text{IV}}$  species in the  $\text{Pb}_3\text{F}_8$  sample and with a small contamination of  $\text{PbF}_2$ , as stated above. The differences in the  $M_5$ -edge itself are more complicated as there are nearly no similarities between the three compounds. In the range from 2500 to 2510 eV,  $\text{PbF}_2$  and  $\text{Pb}_3\text{F}_8$  show similar spectral features, but above that range  $\text{PbF}_2$  exhibits a local minimum, whereas  $\text{Pb}_3\text{F}_8$  shows a peak. A similar peak is observed in the  $\text{Pb}_3\text{O}_4$  spectrum but shifted by nearly 10 eV to higher energies.

We have calculated the electronic structure of  $\text{Pb}_3\text{F}_8$  by DFT methods using the hybrid functional PBE0 and fully relativistic pseudopotentials.<sup>[33,34]</sup> To estimate the accuracy of our calculations we compared the experimentally determined valence band XP spectrum with the calculated partial density of states (pDOS) that is corrected by background and cross-section effects (see the Supporting Information). The results are shown in Figure 5b. The valence band width as well as its three-peaked shape are well reproduced by the DFT calculations.

In the following, we investigate the electronic structure of  $\text{Pb}_3\text{F}_8$  in more detail by calculating its band structure and charge distribution. The band structure as well as the total DOS are given in Figure 6.

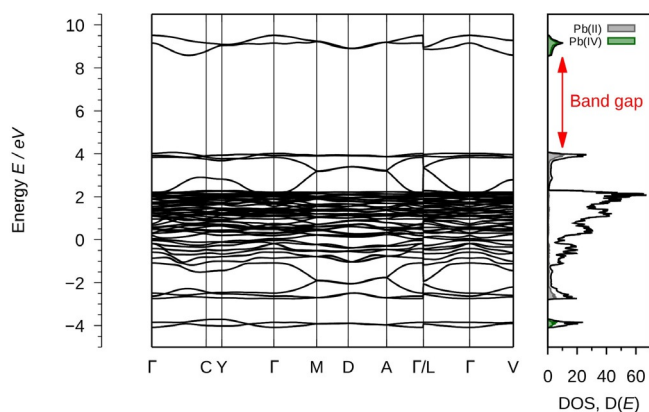


**Figure 6.** Left: Electronic band structure of  $\text{Pb}_3\text{F}_8$ . Right: Total Density of States (DOS) and the projected DOS of the 6s orbitals of  $\text{Pb}^{\text{II}}$  and  $\text{Pb}^{\text{IV}}$ . The position of the band gap (4.5 eV) is highlighted (DFT-PBE0/NCPP with SOC).

The band structure calculations show  $\text{Pb}_3\text{F}_8$  to be an insulator with a band gap of approximately 4.5 eV in line with its off-white color. The DOS of the valence band is dominated by F 2p states that range from  $-1$  eV to 2 eV. At about 4 eV the top of the valence band consists of four bands with only a small amount of dispersion that can be attributed to the filled  $\text{Pb}^{\text{II}}$  6s bands. The conduction band is located at about 9 eV and consists of two bands. Both show nearly exclusive  $\text{Pb}^{\text{IV}}$  6s character as illustrated by the pDOS in the right of Figure 6. A small amount of the  $\text{Pb}^{\text{IV}}$  6s states is located at the bottom of the valence band at about  $-4$  eV due to some covalent  $\text{Pb}^{\text{IV}}\text{-F}$  bond character. For the same reason  $\text{Pb}^{\text{II}}$  6s states are present at about  $-2$  eV. The band structure of the mixed valence compound  $\text{Pb}_3\text{O}_4$  shows similar characteristics.<sup>[11]</sup> We thus conclude

that like  $\text{Pb}_3\text{O}_4$  also  $\text{Pb}_3\text{F}_8$  is a mixed valence compound with the lead atoms in the oxidation states +II and +IV.

The crystal structure of  $\text{Pb}_3\text{F}_8$  indicates that the  $\text{Pb}^{\text{II}}$  atoms feature “sterically active lone-pairs”. We calculated electron-density difference maps of  $\text{Pb}_3\text{F}_8$  which display the difference of the electron density of the compound compared to a superposition of the electron density of free atoms, yielding information where electron density is accumulated or depleted. The electron-density difference map of  $\text{Pb}_3\text{F}_8$  is shown in Figure 7. It is drawn in a view perpendicular to the ladder-like connection of the  $\text{Pb}(2)$  atoms and the  $\text{F}(4)$  atoms, compare Figure 2a.

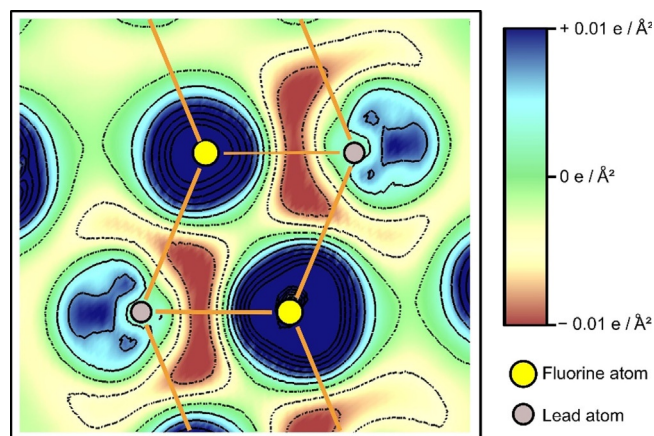


**Figure 7.** Electron-density difference map (DFT-PBE0/NCPP + SOC) of  $\text{Pb}_3\text{F}_8$  along the ladder-like connection (sketched) of the  $\text{Pb}(2)$  atoms (grey color) via  $\mu_2$ -bridging  $\text{F}(4)$  atoms (yellow color). An increase in electron density is shown in blue color and solid black lines, while a decrease in electron density is shown in brown color and dashed black lines.

The map displays a strong polarization of the electron density around the  $\text{Pb}^{\text{II}}$  atoms. The electron density along the  $\text{Pb}\text{-F}$  bonds is minimized (brownish colors) in line with the expected high amount of ionic bonding character. Moreover, there is an accumulation of electron density (in blue colors) besides the  $\text{Pb}^{\text{II}}$  atoms, pointing to the left and right side of the depicted ladder. Therefore, the electron density at the  $\text{Pb}^{\text{II}}$  atoms is “pushed” away from the fluorine atoms inside the ladder. This effect is often referred to “sterically active lone-pairs” of the  $\text{Pb}^{\text{II}}$  atoms. The electron density around the fluorine atoms (in yellow color) is strongly and nearly spherically increased as is expected for  $\text{F}^-$  anions due to the high electronegativity of the F atom.

## Conclusions

The binary lead(II/IV) fluoride  $\text{Pb}_3\text{F}_8$  was synthesized from  $\text{Pb}_3\text{O}_4$  in anhydrous HF at room temperature. The bulk phase appears off-white while single crystals are colorless. It is thermally stable up to circa  $80^\circ\text{C}$  and then decomposes to  $\text{PbF}_2$  under loss of  $\text{F}_2$ . The compound crystallizes in the monoclinic space group  $I2/a$  (No. 15) with the lattice parameters  $a = 8.7800(18)$ ,  $b = 7.4927(15)$ ,  $c = 10.196(5)$  Å;  $\beta = 98.78(3)^\circ$ ;  $V =$

662.9(4) Å<sup>3</sup>; Z=4 at T=100 K, as evidenced by single-crystal X-ray analysis. The description of Pb<sub>3</sub>F<sub>8</sub> as a mixed valence Pb<sup>II</sup>/Pb<sup>IV</sup> compound is evidenced by the thermal decomposition products, the crystal structure, the <sup>19</sup>F solid-state NMR, valence and core level photoelectron, as well as near-edge X-ray absorption fine structure (NEXAFS) spectroscopic investigations and further supported by IR and Raman spectra. Additionally, quantum chemical calculations were carried out to elucidate the electronic structure of Pb<sub>3</sub>F<sub>8</sub>. The calculated band gap is in line with the color of the compound. An accumulation of electron density next to the Pb<sup>II</sup> atoms that some call “sterically active lone-pairs” seems to be responsible for the formation of the peculiar layer structure of Pb<sub>3</sub>F<sub>8</sub>.

## Acknowledgements

We thank the Deutsche Forschungsgemeinschaft for several types of funding (also through 223848855-SFB 1083 and INST 221/117-1 FUGG), Solvay for the generous donation of F<sub>2</sub> and B. Scheibe for the Raman measurement. We thank the analytical service department of Dr. Uwe Linne, Marburg, the Helmholtz-Zentrum Berlin (HZB) for the allocation of synchrotron radiation beamtime at BESSY-II, and Florian Fillsack and Mark Hutter for technical support. We thank Prof. Dr. Michael Ruck, Dresden, for a helpful discussion on “sterically active lone-pairs”.

## Conflict of interest

The authors declare no conflict of interest.

**Keywords:** IR and Raman spectroscopy · lead fluoride · NEXAFS · NMR spectroscopy · quantum chemical calculations

- [1] J. J. Berzelius, *Ann. Phys.* **1824**, *77*, 1–48.  
 [2] B. Brauner, *J. Chem. Soc. Trans.* **1894**, *65*, 393–402.  
 [3] U. Croatto, *Gazz. Chim. Ital.* **1944**, *74/75*, 20–22.  
 [4] R. Hoppe, W. Dähne, *Naturwissenschaften* **1962**, *49*, 254–255.

- [5] P. Charpin, H. Marquet-Ellis, H. Nguyen-Nghi, P. Plurien, *C. R. Seances Acad. Sci., Ser. C* **1972**, *275*, 1503–1506.  
 [6] M. F. A. Dove, R. King, T. J. King, *J. Chem. Soc. Chem. Commun.* **1973**, 944.  
 [7] A. L. Hector, A. Jolleys, W. Levason, D. Pugh, G. Reid, *Dalton Trans.* **2014**, *43*, 14514–14516.  
 [8] J. C. Taylor, P. W. Wilson, *J. Am. Chem. Soc.* **1973**, *95*, 1834–1838.  
 [9] P. Köhler, J.-H. Chang, *Z. Anorg. Allg. Chem.* **1997**, *623*, 596–602.  
 [10] A. Levoll, *Ann. Chim. Phys.* **1840**, *75*, 108–111.  
 [11] H. J. Terpstra, R. A. De Groot, C. Haas, *J. Phys. Chem. Solids* **1997**, *58*, 561–566.  
 [12] E. Van Elslande, V. Guérineau, V. Thirioux, G. Richard, P. Richardin, O. Laprévotte, G. Hussler, P. Walter, *Anal. Bioanal. Chem.* **2008**, *390*, 1873–1879.  
 [13] A. Bose, K. Vashistha, B. J. O’Loughlin, *Pediatrics* **1983**, *72*, 106–108.  
 [14] M. Bannert, G. Blumenthal, H. Sattler, M. Schönherr, H. Wittrich, *Z. Chem.* **2010**, *12*, 191–192.  
 [15] P. Charpin, H. Marquet-Ellis, Nguyen-Nghi, P. Plurien, F. Perrin, *C. R. Seances Acad. Sci., Ser. C* **1972**, *275*, 1503–1506.  
 [16] J. Bandemehr, H. L. Deubner, M. Sachs, F. Kraus, *Z. Anorg. Allg. Chem.* **2018**, *644*, 1721–1726.  
 [17] R. Homann, R. Hoppe, *Z. Anorg. Allg. Chem.* **1969**, *368*, 271–278.  
 [18] H. Hoppe, K. Blinne, *Z. Anorg. Allg. Chem.* **1958**, *293*, 251–263.  
 [19] F. Schrötter, B. G. Müller, *Z. Kristallogr.* **1991**, *196*, 261–268.  
 [20] R. Fischer, B. G. Müller, *Z. Anorg. Allg. Chem.* **2001**, *627*, 445–452.  
 [21] M. Nespolo, B. Guillot, *J. Appl. Crystallogr.* **2016**, *49*, 317–321.  
 [22] K. O. Christe, D. A. Dixon, J. C. P. Sanders, G. J. Schrobilgen, S. S. Tsai, W. W. Wilson, *Inorg. Chem.* **1995**, *34*, 1868–1874.  
 [23] A. Ellern, K. Seppelt, *Angew. Chem. Int. Ed. Engl.* **1995**, *34*, 1586–1587; *Angew. Chem.* **1995**, *107*, 1772–1773.  
 [24] E. J. Baran, *J. Fluorine Chem.* **2000**, *101*, 61–63.  
 [25] R. Seshadri, *J. Chem. Sci.* **2001**, *113*, 487–496.  
 [26] A. Walsh, G. W. Watson, *J. Solid State Chem.* **2005**, *178*, 1422–1428.  
 [27] J. Köhler, J. Tong, R. Dinnebier, A. Simon, *Z. Anorg. Allg. Chem.* **2012**, *638*, 1970–1975.  
 [28] F. Wang, C. P. Grey, *J. Am. Chem. Soc.* **1998**, *120*, 970–980.  
 [29] M. Bak, J. T. Rasmussen, N. C. Nielsen, *J. Magn. Reson.* **2000**, *147*, 296–330.  
 [30] M. Robin Bendall, R. E. Gordon, *J. Magn. Reson. (1969-1992)* **1983**, *53*, 365–385.  
 [31] Y. S. Avadhut, J. Weber, E. Hammarberg, C. Feldmann, I. Schellenberg, R. Pöttgen, J. Schmedt auf der Günne, *Chem. Mater.* **2011**, *23*, 1526–1538.  
 [32] B. Bureau, G. Silly, J. Y. Buzaré, J. Emery, *Chem. Phys.* **1999**, *249*, 89–104.  
 [33] C. Adamo, V. Barone, *J. Chem. Phys.* **1999**, *110*, 6158–6170.  
 [34] M. Schlipf, F. Gygi, *Comput. Phys. Commun.* **2015**, *196*, 36–44.

Manuscript received: August 29, 2019

Accepted manuscript online: September 23, 2019

Version of record online: November 4, 2019